LEGIBILITY NOTICE

A major purpose of the Technical Information Center is to provide the broadest dissemination possible of information contained in DOE's Research and Development Reports to business, industry, the academic community, and federal, state and local governments.

Although a small portion of this report is not reproducible, it is being made available to expedite the availability of information on the research discussed herein.

Los Alamos National Laboratory is operated by the University of California for the United States Department of Energy under contract W-7405-ENG-36

LA-UR--88-153

DE88 005386

TITLE FRAGMENTATION AND FLOW IN CENTRAL COLLISIONS

AUTHOR(S) B. V. Jacak, K. G. R. Doss, H.-A. Gustafsson, H. Gutbrod, J. W. Harris, K.-H. Kampert, B. Kolb, A. M. Poskanzer, H. G. Ritter, H. R. Schmidt, L. Teitelbaum, M. Tincknell, S. Weiss, and H. Wieman

SUBMITTED TO Texas A&M Symposium on Hot Nuclei, College Station, TX, December 7-10, 1987

DISCLAIMER

Los Alamos National Laboratory
Los Alamos, New Mexico 87545

FRAGMENTATION AND FLOW IN CENTRAL COLLISIONS

B. V. Jacak,[a] K.G.R. Doss,[b] H.-A. Gustafsson,[c] H. Gutbrod,[*] J.W. Harris,[**] K.-H. Kampert,[***] B. Kolb,[*] A.M. Poskanzer,[**] H.G. Ritter,[**] H.R. Schmidt,[*] L. Teitelbaum,[**] M. Tincknell,[**] S. Weiss,[**] and H. Wieman[**]

There has been considerable recent interest in the production of medium mass fragments (A>4) in intermediate and high energy nucleus-nucleus collisions. The mechanism for production of these fragments is not well understood; attempts to describe fragmentation employ a variety of assumptions. Some examples are: disassembly of a system in thermal equilibrium into nucleons and nuclear fragments,[1,2] liquid-vapor phase transitions in nuclear matter,[3] final state coalescence of nucleons[4] and dynamical correlations between nucleons at breakup.[5,6] Single particle inclusive measurements are inadequate to distinguish among the models, as the fragment mass (or charge) distributions are well described by all. Even the basic question whether the fragments arise from "hot" or "cold" matter has not yet been answered.

Investigation of the fragmentation mechanism requires the measurement of more complicated observables. To identify what part of the reacting system gives rise to the fragments, it would be useful to tag them as participants or spectators. Such a separation is far from clearcut, and information about the impact parameter of the collision is crucial. A large acceptance for all the reaction products and an event-by-event measurement

[a] Los Alamos National Laboratory, Los Alamos, NM 87545.
[b] Present address: Linear Accelerator Laboratory, University of Saskatchewan, Saskatoon, Saskatchewan, Canada S7N OWO.
[c] Present address: University of Lund, Solvegaton 14, S-22362 Lund, Sweden.
[*] Gesellschaft für Schwerionenforschung, Darmstadt, West Germany.
[**] Lawrence Berkeley Laboratory, University of California, Berkeley, CA 94720.
[***] Permanent address: University of Münster, D-4400 Münster, West Germany.

of the fragment multiplicity is required to distinguish fragment formation via sequential emission from a large equilibrated system and multifragmentation. In order to address whether fragments are formed early or late in the collision, information about the dynamical evolution of the reaction is necessary. This can be provided by study of the global properties of the events.

Analysis of global variables can also allow us to extend recent studies of collective sidewards flow of light particles.[7,8] Collective flow was initally predicted by theoretical fluid dynamics,[9,10,11] but also arises in various other models[12,13,14,15] incorporating compressional degrees of freedom in the form of a pressure-density relation, i.e., an equation of state. In these models the amount of transverse flow is directly related to the stiffness of the nuclear equation of state and transport properties of the nuclear medium.[16] At non-zero impact parameters there is an inherent asymmetry in the pressure developed in the interaction region, which results in a transverse flow of matter in the direction of lowest pressure. Several calculations[17,18,19] capable of producing nuclear fragments predict that a stronger collective flow effect should be observed for the fragments than for light particles emitted in the reaction. Additionally, the presence of the effect in detected fragments may provide further clues to their production mechanism.

The GSI/LBL Plastic Ball/Wall detector system[20] was used to study light and intermediate mass fragments over a large solid angle in 200 MeV/nucleon Au + Au reactions at the Bevalac. The detector layout is shown in Fig. 1.

The Plastic Ball consists of 815 $CaF_2(\Delta E)$-Plastic Scintillator(E) telescope modules covering the angular region from $10° \leq \theta_{lab} \leq 160°$ with H and He isotope identification. Computer-controlled high voltage modules were implemented on the 160 Ball modules at $\theta_{lab} \leq 30°$ to enable online gain-matching. With a careful reduction in gain for these forward Ball modules, their dynamic range was extended, enabling the simultaneous measurement of all produced nuclei from H to Ne. Unit separation of nuclear charges for $1 \leq Z \leq 10$ was obtained with isotope separation for Z = 1 and 2. A calibration for the fragment charge identification was made by detecting low energy ^{12}C beams and ^{12}C fragmentation products at the Bevalac using time-of-flight techniques. In order to be identified, fragments were required to traverse the 4 mm thick CaF_2 scintillator producing a low energy cut-off in the laboratory of $E_{lab} \approx$ 35-40 MeV/nucleon. Since the velocity of the c.m. system corresponds to $E_{lab} \approx$ 50 MeV/nucleon, the low energy cut-off is not important in the forward direction of the c.m. system. The measurements

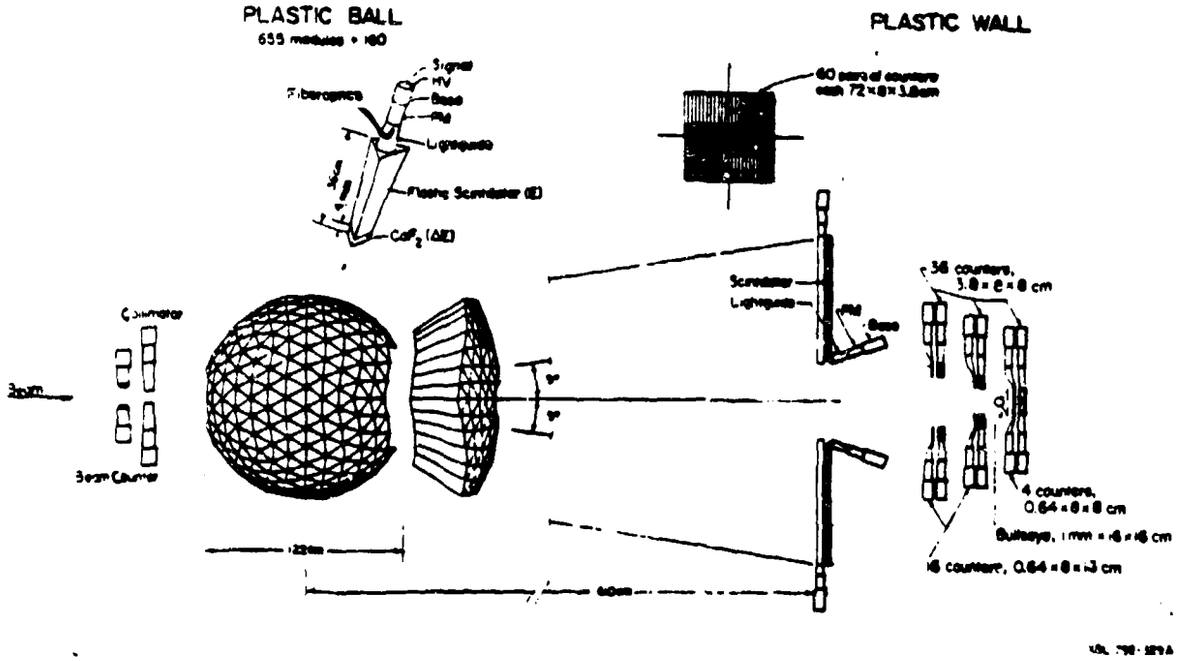

Fig. 1. Schematic view of the Plastic Ball and the Plastic Wall.

of intermediate mass fragments were only performed at $\theta_{lab} \leq 30°$, which corresponds to the forward hemisphere in the c.m.

The Plastic Wall covers angles $\theta_{lab} \leq 10°$ with 60 pairs of scintillation counters, providing particle identification for $1 \leq Z \leq 6$ and velocities $\beta \geq 0.3$ (45 MeV/nucleon) via time-of-flight and energy loss. The acceptance for light charged particles extends over 4π, allowing each event to be characterized by charged particle multiplicity. In addition, there was a zero degree gas proportional chamber[21] cover $0 \pm 2°$ in the laboratory. This detector with its five wire planes enabled extremely high position resolution for large projectile remnants. Beam defining counters employing standard pile-up rejection techniquies were used to ensure against chance coincidence events.[20]

The observed participant charge multiplicity distribution for Au + Au is shown in Fig. 2. We have used this quantity to sort the events into groups according to impact parameter, as indicated by the lines in the figure. The events with the fewest observed charges (labeled "MUL1") correspond to the most peripheral collisions, while the events with the highest charge multiplicities ("MUL5") arise from central collisions. The drop in the number of events with very low multiplicities is a result of the trigger used in the experiment, which was designed to discriminate against the most peripheral collisions.

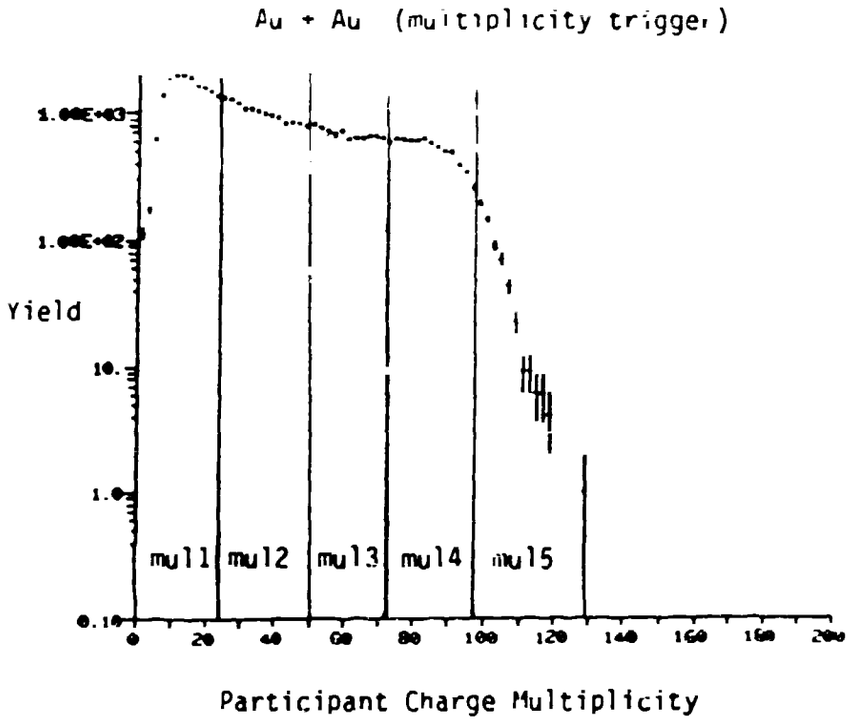

Fig. 2. Participant charge multiplicity distribution for 200 MeV/n Au + Au. This includes protons bound in H and He isotopes.

Figure 3 shows a density plot of the invariant cross section for lithium fragments from Au + Au, as a function of the rapidity and the perpendicular momentum per nucleon. The five parts of the figure correspond to the five cuts on the participant charge multiplicity indicated in Fig. 2. No corrections for the angular and energy cutoffs in the detector have been applied to the data. Thus two distinct sections are visible in each plot, corresponding to the two subsections of the detector system which were sensitive to intermediate mass fragments.

It is evident from the figure that peripheral collisions give rise to fragments with rapidities very close to the beam rapidity, consistent with expectations for fragmentation of a slightly excited projectile. In the "MUL1" plot we see a hole in the yield at exactly the beam rapidity, corresponding to coulomb repulsion between the emitted lithium fragment and a heavy remnant of the Au projectile. In events where a projectile remnant is observed, the azimuthal angles of the remnant and fragments are correlated, supporting the picture of fragments evaporated from a large projectile residue.

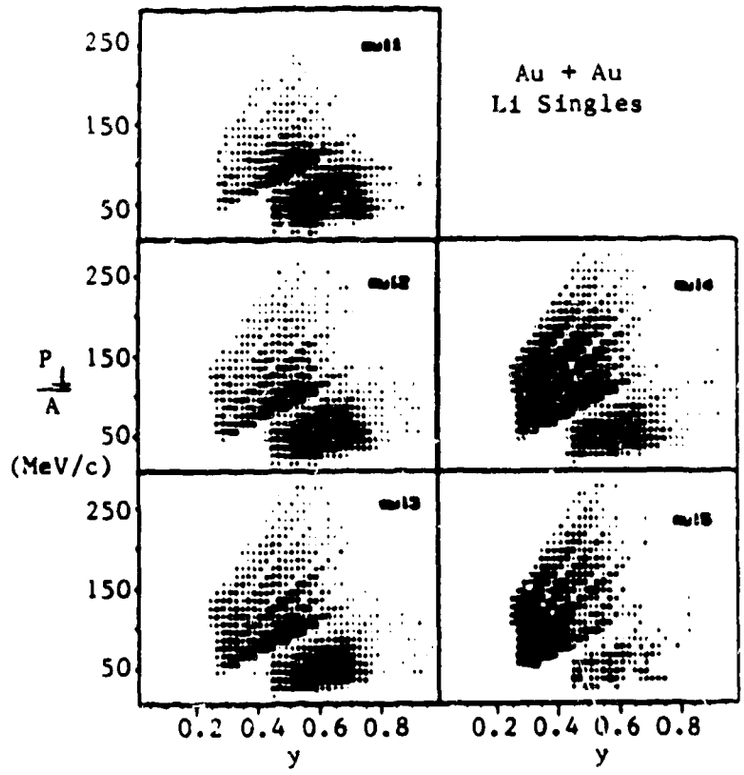

Fig. 3. Multiplicity selected rapidity plots for lithium fragments from Au + Au. The multiplicity bins range from lowest (MUL1), indicating peripheral collisions to highest (MUL5), containing central collisions.

In the more central collisions in the highest multiplicity bins, we see many lithium fragments emitted with smaller rapidities, intermediate between those of the target and the projectile. In contrast to the forward peaked angular distributions arising from peripheral collisions, these fragments are emitted relatively isotropically in the center of mass system. Such behavior is what one might expect when the projectile nucleons impart more energy to the target and create an excited region which moves at a velocity approximately halfway between that of the projectile and the target.

The transition between the peripheral and central collisions is very smooth, with a gradual shift in the rapidities of the observed fragments away from the projectile rapidity. In order to check if both projectile-like and midrapidity fragments are formed in the same event, we chose events with multiple fragments and required that at least one fragment fall into a midrapidity window. We made a rapidity plot similar to Fig. 3 of the other

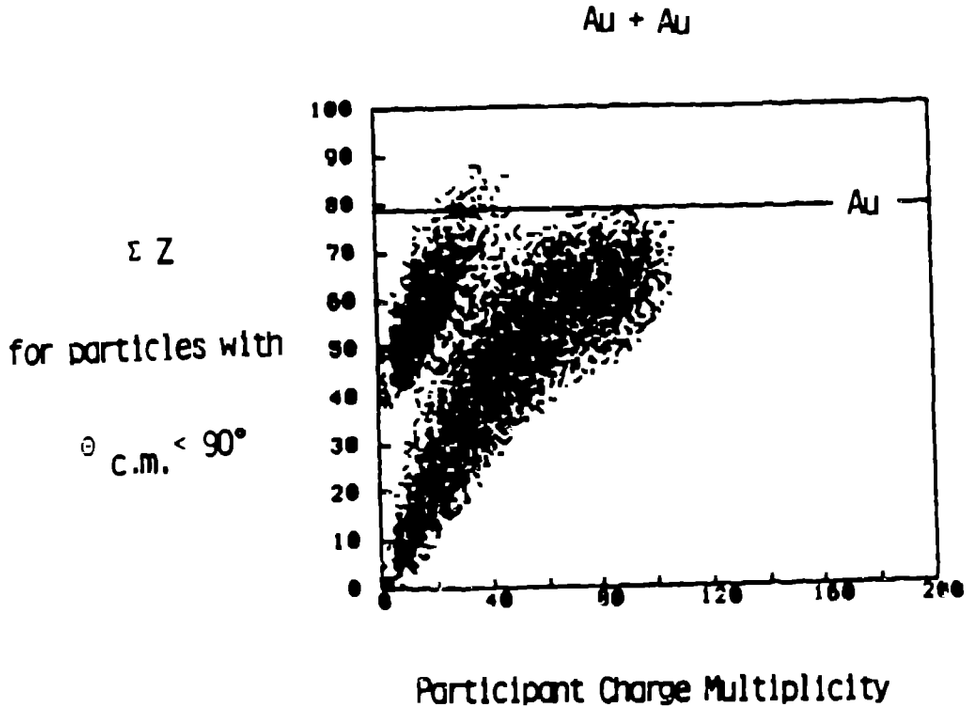

Fig. 4. Sum of charges observed in the forward c.m. hemisphere, as a function of the participant charge multiplicity. The separate lobe at low multiplicity corresponds to events with a large projectile remnant detected at very forward angles.

fragments in the event, and found that the mixing occurs event-by-event· even in the central collisions where midrapidity fragments are formed, we observe some associated projectile rapidity fragments.

In order to look for multifragmentation events, and to understand the breakup of the system as a function of impact parameter, we summed the charges observed in the forward c m. hemisphere and compared this with the charge of one Au nucleus. The resulting sum is shown in Fig. 4, plotted as a function of the participant charge multiplicity. For peripheral collisions, a large projectile remnant in detected in many events; these correspond to the small lobe on the left (low multiplicity) side of the figure. The charge of the projectile remnant is not well determined, so it is assigned one half the charge of the projectile. It is clear that this procedure underestimates the remnant charge for the most peripheral collisions and overestimates it as the impact parameter and projectile remnant become smaller. The low multiplicity section in the large lobe in the figure corresponds

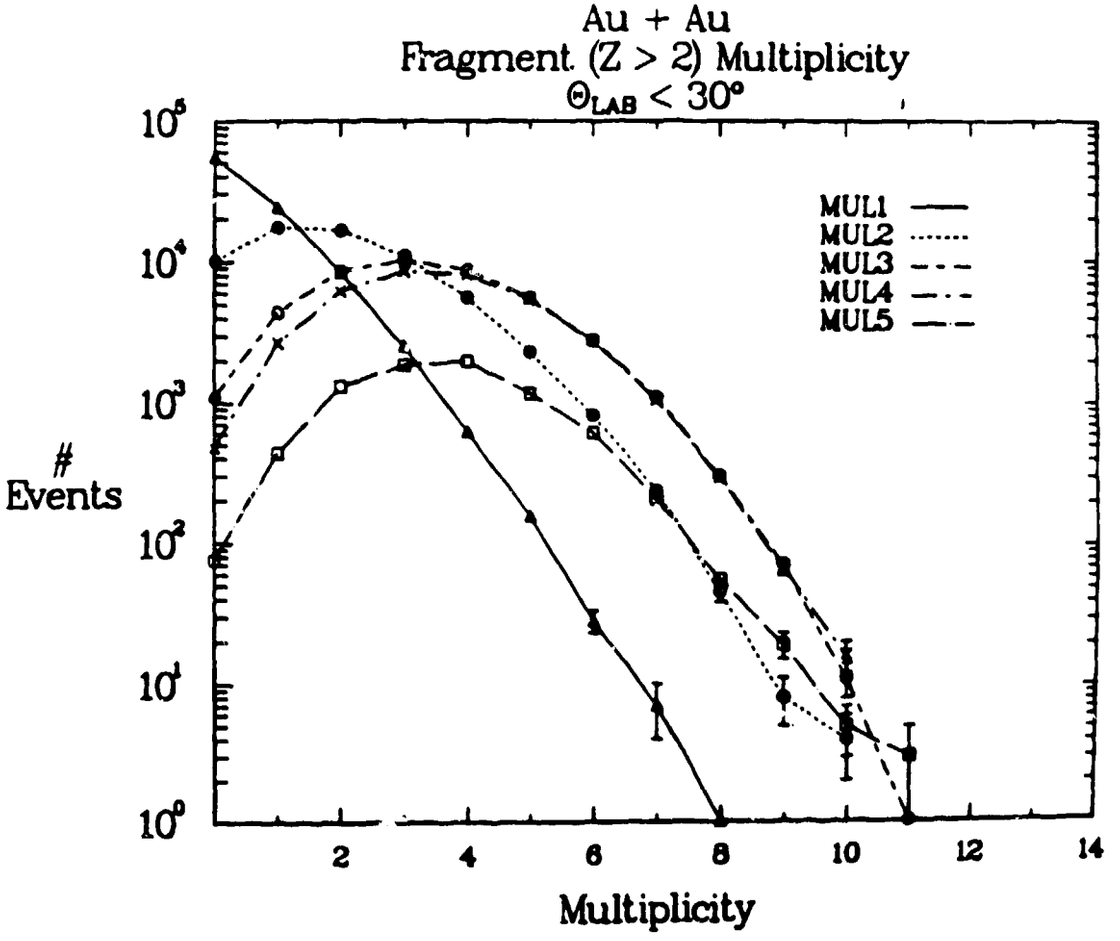

Fig. 5. Fragment ($Z > 2$) multiplicity distributions for 200 MeV/n Au + Au for five participant charge multiplicity bins increasing from MUL1 to MUL5. These multiplicities correspond to fragments emitted in the forward hemisphere of the c.m. system.

to events where the projectile remnant was not recorded in the zero degree chamber.

For central collisions (large multiplicities), nearly all of the Au charge is observed in the form of light and intermediate mass fragments. These results indicate that in central and near-central collisions the system breaks up into small and medium mass fragments ($Z \leq 10$) with no large nuclear remnant. As well as indicating the onset of multifragmentation, Fig. 4 also illustrates the high efficiency of the detector system and motivates an event-by-event study of the fragment multiplicities.

Multiplicity distributions of fragments with $3 \leq Z \leq 10$, observed in the forward hemisphere in the c.m. frame are shown in Fig. 5. The events are sorted according to the participant charge multiplicity into five bins. Most peripheral collisions (MUL1) result in

a low multiplicity of intermediate mass fragments. These fragments have energies close to that of the projectile and are usually accompanied by a large projectile remnant. In more central collisions (MUL4 and MUL5) where practically all of the projectile charge is observed in light and intermediate mass fragments, there are on average 3-4 fragments per event at $\theta_{cm} \leq 90°$. Extrapolation to 4π leads to 8 or more intermediate mass fragments in central collisions, with a significant number of events producing as many as 20 fragments. These numbers are slight underestimates due to the low beta cut-off for fragments.

The large number of fragments formed in central collisions, and their emission at midrapidity, motivate analysis of global variables to study the dynamics of the collision and the fragmentation mechanism. To investigate whether the collective flow effect present in light particles is also exhibited by heavier fragments, the transverse momentum analysis technique[22] was employed to determine the reaction plane of each event. In this method the vector difference of the transverse momentum components of particles going forward and those going backwards in the c.m. is used together with the beam axis to define the reaction plane. This difference corresponds to the collective transverse momentum transfer in the c.m. The transverse momentum pperp of each particle is then projected onto the reaction plane, where the particle of interest has been excluded from determination of the plane (i.e. autocorrelations are removed), yielding the inplane transverse momentum p_x. For each particle the fraction of the particle's transverse momentum that lies in the reaction plane is calculated.

Displayed in Fig. 6 is the mean value of the transverse momentum alignment $\langle p_x/p_\perp \rangle$ in the MUL3 multiplicity bin for particles as a function of their rapidity for Z=1,2,3 and 6. Positive and negative values of $\langle p_x/p_\perp \rangle$ correspond to emission projected into the reaction plane, but on opposite sides. The forward-backward asymmetry is an artifact of experimental biases at low particle energies (near target rapidity) and spectator cuts in the projectile rapidity region made using the prescription of Ref. 23. Since participant-spectator discrimination is not unique, the slopes of the curves at midrapidity in Fig. 6 best characterize the flow.[24] It is clear that an increasingly larger part of the fragment's transverse momentum lies in the reaction plane as the fragment mass increases. The Z = 3,6 fragments are more aligned in the plane than the Z = 1,2 particles, which are interpreted to flow collectively.[7,8,12,13,14,15,22]

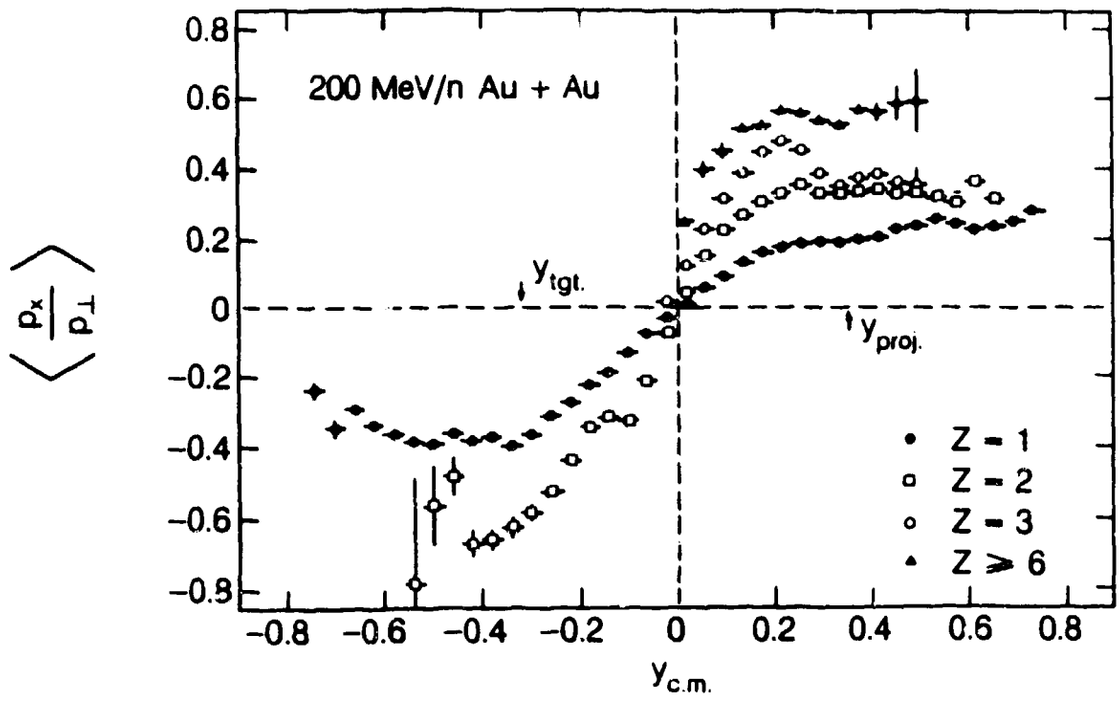

XBL 877-11115

Fig. 6. The mean value of the transverse momentum projected onto the reaction plane (defined in text) divided by the transverse momentum vector modulus as a function of c.m. rapidity for 200 MeV/n Au + Au. Shown are the values for Z = 1,2,3 and Z ≥ 6.

Having studied the alignment of fragments in momentum space, the spatial correlation of the fragments with the reaction plane will now be examined. Presented in Fig. 7 are directivity plots showing the azimuthal correlation of emitted light particles and fragments with the reaction plane. The angle plotted is the azimuthal emission angle of each particle or fragment with respect to the reaction plane defined by the Z = 1,2 particles with autocorrelations removed. The left-hand column labeled MUL2 contains relatively peripheral collisions, and the right, MUL4, relatively central ones. Collisions at extremely large or small impact parameters result in poorly-defined reaction planes and are not shown here. The two curves in each box correspond to rapidities of the emitted particles and fragments: near-midrapidity $0.32 < y < 0.42$ (circles) and near-projectile rapidity $0.52 < y < 0.62$ (crosses), where the projectile rapidity is 0.64. A strong azimuthal correlation is observed between all $Z \geq 2$ nuclei and the azimuthal direction of

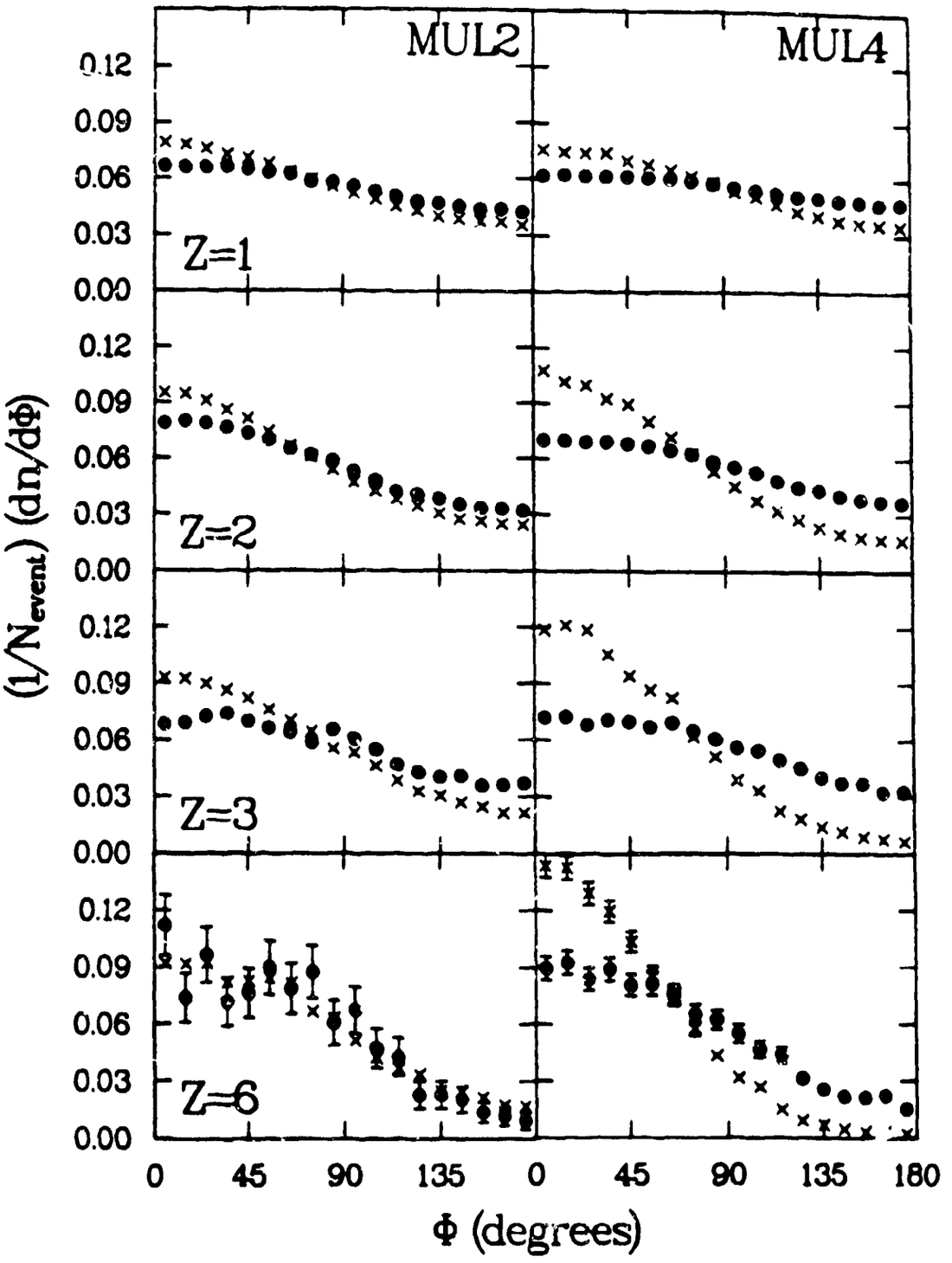

Fig. 7. Directivity plots (azimuthal angular correlations) for Z = 1,2,3 and 6 relative to the azimuthal direction of maximum collective momentum transfer in the flow plane. The left-hand column contains peripheral collisions and the right-hand column relatively central ones. The data are plotted for two rapidity intervals: circles: $0.32 < y < 0.42$ and crosses: $0.52 < y < 0.62$.

maximum collective momentum transfer in the flow plane $\phi = 0$. The correlation is rather flat for Z=1 and becomes increasingly stronger for heavier fragments. Projectile rapidity fragments are more correlated than midrapidity ones. The effect on projectile rapidity fragments is larger in central collisions than peripheral ones, whereas the midrapidity fragment correlations have very little dependence upon the centrality of the collision. In the limit of complete thermalization, azimuthally symmetric emission of midrapidity particles is expected. However, the presence of a correlation between fragments and the reaction plane suggests that this picture is too simple; dynamic compression-expansion effects are present for the midrapidity fragments and high multiplicity (central) events.

The observed correlations are predicted to arise from collective flow of matter in the collision. This should be more important for central collisions than peripheral ones, and a stronger correlation is indeed seen on the right side of Fig. 7. The mass dependence of the correlation is also consistent with predictions of flow.[17,18,19] One might expect that the correlations from collective motion will be somewhat reduced by the random thermal motion generated in such energetic collisions. However, this is not always the case. For a system of nucleons and fragments in thermal equilibrium at a fixed freezeout temperature, the thermal energy is equally partitioned. Thus, the thermal energy per nucleon in a fragment of mass A has a 1/A dependence. The flow energy, which is originally compressional energy built up in the early stages of the collision, should have a linear A dependence, i.e. the compressional energy per nucleon is independent of A. Since the final fragment energy is a sum of the thermal and flow energies, the flow is an increasingly larger fraction of the fragment energy and the thermal energy less important as the fragment mass increases. Figure 8 shows the mean transverse momentum in the reaction plane per nucleon ($\langle p_x/A \rangle$) for light and medium mass fragments, as a function of their rapidity. If the flow energy were to dominate the particle motion, the curves would lie on top of one another. They are in fact close, though not quite overlapping, consistent with the expectation of some random thermal motion. The slightly stronger correlation with the reaction plane for the heavier fragments indicates that the thermal energy does indeed become less important as the fragment mass increases.

Results from the first large solid angle measurement of fragment formation in peripheral and central heavy ion collisions have been presented. The events are characterized through 4π measurement of the light charged particles, yielding impact parameter information and allowing identification of multifragmentation events and analysis of the flow of

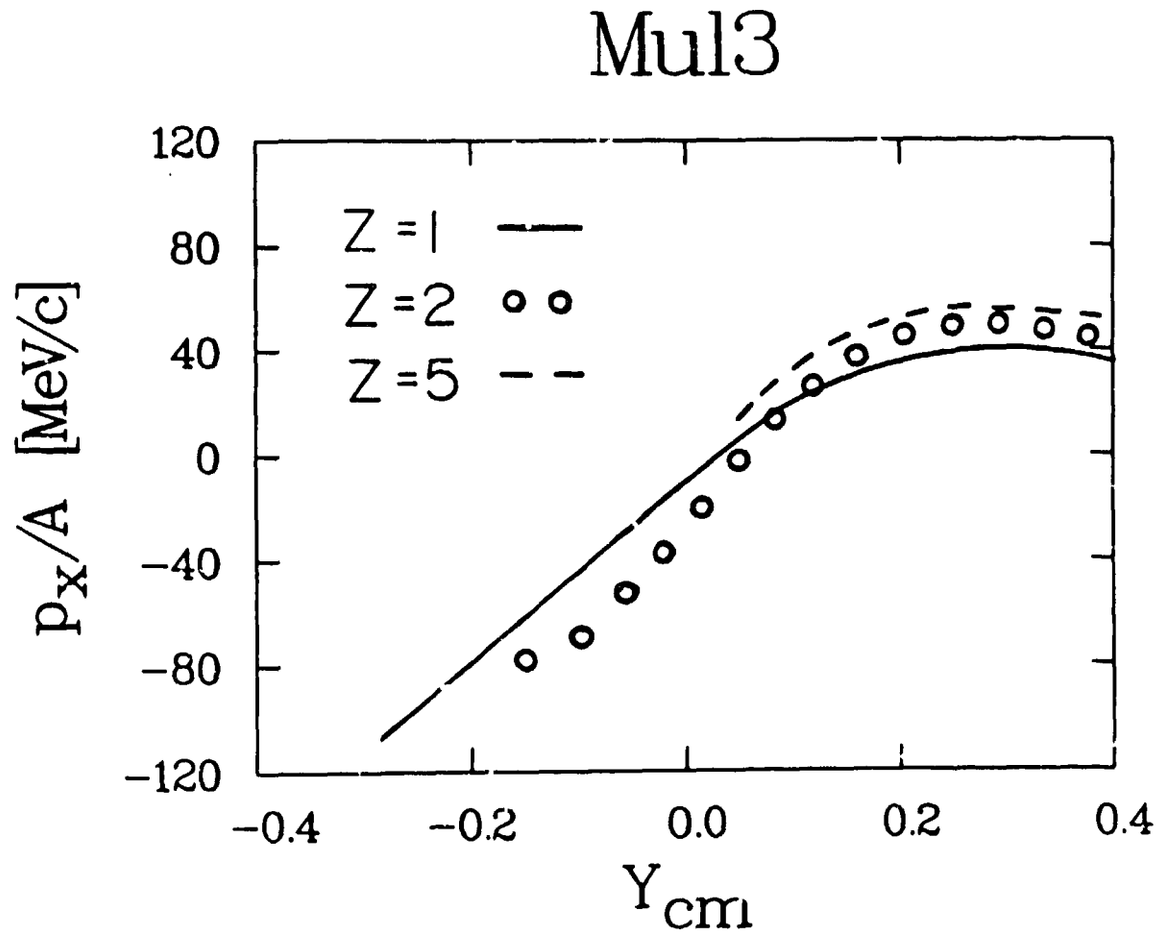

Fig. 8. The mean value of the transverse momentum per nucleon projected onto the reaction plane, as a function of c.m. rapidity. The curves are for Z = 1,2 and 5.

the emitted nucleons and nuclear fragments. On average, 8-9 intermediate mass fragments ($2 \leq Z \leq 10$) are produced in central Au + Au collisions at 200 MeV/nucleon, with up to 20 observed in some events. The transverse momentum per nucleon characterizing the flow and the alignment of the fragments both in position and momentum space relative to the reaction plane is observed to increase with the mass of the fragment, supporting theoretical predictions of the existence of an enhanced collective flow of heavier nuclear fragments. The flow data alone may not allow us to distinguish production of fragments in equilibrium models from coalescence of nucleons, since the A dependence in both approaches is the same.[35] However, it does tell us that the fragment formation mechanism

preserves dynamical information from the early stages of the collision, and provides a more sensitive probe for future studies of the nuclear matter equation of state.

REFERENCES

1. J. Randrup and S. E. Koonin, Nucl. Phys. A356, 223 (1981). G. Fai and J. Randrup, Nucl. Phys. A404, 551 (1983).

2. J. P. Bondorf, R. Donangelo, I. N. Mishustin, C. J. Pethick and K. Sneppen, Phys. Lett. 150B, 57 (1985).

3. G. Bertsch and P. J. Siemens, Phys. Lett. 126B, 9 (1983).

4. H. H. Gutbrod, A. Sandoval, P. Johansen, A. M. Poskanzer, J. Gosset, W. G. Meyer, G. D. Westfall, and R. Stock, Phys. Rev. Lett. 37, 667 (1976).

5. B. Strack and J. Knoll, Z. Phys. A315, 249 (1984).

6. G. E. Beauvais, and D. H. Boal, Univ. of Ill. preprint P/86/2/26, 1986.

7. H.-A. Gustafsson, H.H. Gutbrod, B. Kolb H. Löhner, B. Ludowigt, A.M. Poskanzer, T. Renner, H. Riedesel, H.-G. Ritter, A. Warwick, F. Weik and H. Wieman, Phys. Rev. Lett. 52 1590 (1984).

8. R.E. Renfordt, D. Schall, R. Bock, R. Brockman, J.W. Harris, A. Sandoval, R. Stock, H. Ströbele, D. Bangert, W. Rauch, G. Odyniec, H.G. Pugh and L.S. Schroeder, Phys. Rev. Lett. 53 763 (1984)

9. W. Scheid, H. Mueller and W. Greiner, Phys. Rev. Lett. 32 741 (1974).

10. A.A. Amsden, G.F. Bertsch, F H. Harlow and J.R. Nix, Phys. Rev. Lett. 35 905 (1975).

11. H.Stöcker, J. Maruhn and W. Greiner, Phys. Rev. Lett. 44 725 (1980).

12. H. Kruse, B.V. Jacak and H. Stöcker, Phys. Rev. Lett 54 (1985) 289.

13. J. Aichelin and H. Stöcker, Phys. Lett. 176 14 (1986).

14. R.Y. Cusson, P.G. Reinhardt, J.J. Molitoris, H. Stöcker, M. Strayer, and W. Greiner, Phys. Rev. Lett. 55 2786 (1985).

15. C. Gale, G. Bertsch and S. DasGupta, Phys. Rev. C35 1666 (1987).

16. G.F. Bertsch W.G. Lynch and M.B. Tsang, Phys. Lett. B189 384 (1987).

17. H. Stöcker, A.A. Ogloblin and W. Greiner, Z. Phys. A303 259 (1981).

18. L.P Csernai, H. Stöcker, P.R. Subramanian, G. Graebner, A. Rosenhauer, G. Buchwald, J.A. Maruhn and W. Greiner, Phys. Rev. C28 2001 (1983).

19. L.P. Csernai, G. Fai and J. Randrup, Phys. Lett. 140B 149 (1984).

20. A. Baden, H.H. Gutbrod, H. Löhner, M.R. Maier, A.M. Poskanzer, T. Renner, H. Riedesel, H.G. Ritter, H. Spieler, A. Warwick, F. Weik and H. Wieman, Nucl. Inst. and Meth. 203, 189 (1982).

21. R. Albrecht, H.W. Daues, H.A. Gustafsson, H.H. Gutbrod, K.H. Kampert, B.W. Kolb, H. Löhner, B. Ludewigt, A.M. Poskanzer, H.G. Ritter, R. Schulze, H. Stelzer and H. Wieman, Nucl. Inst. and Meth. A245 82 (1986).

22. P. Danielewicz and G. Odyniec, Phys. Lett. 157B 146 (1985).

23. K.G.R. Doss, H.A. Gustafsson, H.H. Gutbrod, B. Kolb, H. Löhner, B. Ludewigt, A.M. Poskanzer, T. Renner, H. Riedesel, H.G. Ritter, A. Warwick and H. Wieman, Phys. Rev. C32 116 (1985).

24. K.G.R. Doss, H.-A. Gustafsson, H.H. Gutbrod, K.-H. Kampert, B. Kolb, H. Löhner, B. Ludewigt, A.M. Poskanzer, H.G. Ritter, H.R. Schmidt and H. Wieman, Phys. Rev. Lett. 57 382 (1986).

25. J. Gosset, H.H. Gutbrod, W.G. Meyer, A.M. Poskanzer, A. Sandoval, R. Stock and G.D. Westfall, Phys. Rev. C16 629 (1977).